CrystEngComm

PAPER

View Article Online
View Journal | View Issue

Cite this: *CrystEngComm*, 2015, **17**, 3695

Critical size for the β- to α-transformation in tin nanoparticles after lithium insertion and extraction†

N. Oehl,* L. Hardenberg, M. Knipper, J. Kolny-Olesiak, J. Parisi and T. Plaggenborg

Received 22nd January 2015,
Accepted 16th March 2015

DOI: 10.1039/c5ce00148j

www.rsc.org/crystengcomm

Tin nanoparticles can be transformed from the metallic β-Sn structure to the semiconducting α-Sn structure after electrochemical lithiation and delithiation at room temperature. Here, we studied the influence of the size of the crystallites on the β- to α-transformation in Sn nanoparticles. Differently sized Sn/SnO_x nanoparticles were synthesized, processed in electrodes and cycled ten times in a lithium-ion cell at room temperature. X-ray diffraction (XRD) patterns before and after electrochemical lithium insertion/extraction reveal that samples with small particles contain the α-Sn structure. The critical size for this transformation is 17(4) nm. Smaller particles were transformed into the α-Sn structure while particles larger than 17 nm retain the β-Sn structure. Temperature dependent XRD measurements show that this α-Sn structure is stable up to 220 °C before its reflections disappear. The formation of the α-Sn structure at room temperature in small particles and the unexpected high transition point can be explained by the substantial contribution of the surface energy (facilitating formation of alloys not observed in the bulk), lithium impurities in the α-Sn structure and the Li_2O shell which is formed during lithium insertion.

Introduction

Fundamental properties and behaviors of nanoparticles are determined by their size. Lattice parameters[1,2] and even the crystal structure[3] itself can change, depending on the size of the crystallite. Size-induced phase transformation in nanoparticles was investigated for several oxides *e.g.* TiO_2,[4] Y_2O_3,[5] Al_2O_3 [6] and even in metals like Co,[7] Ag[8] or Au.[9] Tin, and tin nanoparticles in particular, has been tested as a high-charge anode material in lithium-ion batteries, because it provides a three times higher charge density than the commonly used graphite.[10] The size effect on the cycling stability[11] as well as different surface modifications[12] were tested to enhance stability and power. *In situ* XRD measurements of tin bulk electrodes disclose that the lithiation process of tin follows defined Li–Sn-phases.[13] But detailed studies about the changes of the nanoparticle crystal structure during lithium insertion/extraction have not been reported yet.

The formation of the α-Sn structure in tin nanoparticles after cycling in a lithium-ion battery anode was reported previously,[12,14,15] however, this phenomenon was not investigated further. A lot of research is focusing on the formation of the semiconducting α-Sn in lead free solders.[16,17] This transformation is also called tin pest. Plumbridge[18] reported the formation of tin pest in several new-generation lead-free solder alloys when exposed to temperatures below the allotropic transition point for tin (<13 °C). It has been demonstrated that small amounts (0.5 wt%) of Si[19] and Ge[20] can stabilize the α-phase, while Cu or Pb[21] stabilize the β-phase. A phase transformation of the β- to α-structure at room temperature was not observed. Fyhn *et al.*[19] reported that small Sn precipitates in a Si matrix can form stable α-Sn structures with a melting point at 200 °C.

In this study, we investigate the size-dependent transformation of the β- to α-Sn structure at room-temperature. In our previous study we found that small (~10 nm) β-Sn nanoparticles can be transformed into the α-Sn structure, while larger (~80 nm) particles retain the β-phase when cycled in a lithium-ion cell at room temperature.[12] The goal of our present study is, to determine the critical size at which Sn nanoparticles undergo this structural change. Therefore, we prepared Sn nanoparticles with different sizes and cycled them in a lithium-ion cell. These cells were studied by XRD to determine the weight ratio between the β- and α-phase. By

Energy and Semiconductor Research Laboratory, Institute of Physics, Carl-von-Ossietzky Universität, Carl-von-Ossietzky-Str. 9-11, 26129 Oldenburg, Germany. E-mail: nikolas.oehl@uni-oldenburg.de

† Electronic supplementary information (ESI) available: Potential *vs.* specific capacity profiles and corresponding differential capacity plots of the 15 nm nanoparticle sample and specific lithiation capacity *vs.* cycle number for the constant-current–constant-potential charge/discharge cycles of some investigated nanoparticle electrodes with different particle sizes. See DOI: 10.1039/c5ce00148j

comparison of these data with the size distribution of the original particles obtained from TEM we calculated the critical size for this transformation.

Experimental methods

Different-sized Sn/SnO_x core/shell nanoparticles were synthesized *via* a chemical reduction method from 15 nm to 80 nm. Detailed synthesis parameters where described in our earlier work.[2] These particles were dispersed in water with sodium carboxymethyl cellulose (CMC, Sigma Aldrich) and conductive carbon black (Super P 99+% Alfa Aesar) with 80 wt% active material, 10 wt% binder and 10 wt% carbon. The slurry was drop-casted on punched (1.2 cm diameter) cupper foil (2 mg active material) and dried in an oven at 75 °C for 5 hours. The electrodes were stored in a nitrogen glovebox with water and oxygen vapor contents below 10 ppm.

Electrical measurements were performed in lab-scale Swagelok cells with two-electrode configurations. Metallic lithium foil (Alfa Aesar, 0.75 mm thick, 99.9%) was used as a counter (D = 12 mm) electrode. Battery grade 1 M $LiPF_6$ EC/DMC 50 : 50 (v/v) solution (Sigma Aldrich) was used as electrolyte. All cells were assembled in an argon filled glovebox.

Charge/discharge cycling was performed on a Keithley SourceMeter 2600 Unit. The cycling procedure for all the Sn-anodes consisted of constant-current–constant-voltage steps (10 times), starting with constant current step (0.1 mA cm^{-2}). The operating potential range was set between 2 V and 0.005 V *versus* Li/Li^+. At every cut-off potential the voltage was set constant for 30 min. All experiments were carried out at room temperature.

XRD measurements on the Sn electrodes were performed before and after cycling using a PANalytical X'Pert Pro diffractometer operating with CuKα radiation in Bragg–Brentano θ–2θ-geometry, using a goniometer with 240 mm radius and an automatic divergence slit. A standard reference material (660b La_6) from the National Institute of Standards and Technology (NIST) was used to refine the instrumental line broadening parameters. Peak parameters (position, intensity, integral breath) were collected by fitting two (Kα_1 and Kα_2) pseudo Voigt functions on all reflections from the pattern, using the High Score Plus (3.0.5.) software. All nanoparticle electrodes were deposited on low background silicon sample holders and sealed under Kapton foil to prevent oxidation.

Temperature dependent XRD measurements were carried out in an argon-flowed heating chamber (HTK1200N/Anton Paar) using an Al_2O_3 sample holder, a Kanthal APM (72.2% Fe, 22% Cr, 5.8% Al) heating element and a Pt-10%Rh-Pt sensor (type S) thermocouple. The temperature was stabilized at each measurement (accuracy ± 2 °C) for 15 min. XRD Theta–2Theta scans were collected every 10° starting at room temperature with measurement duration of 60 min for each scan.

Transmission electron microscopy (TEM) measurements were carried out using a Zeiss EM 902A microscope with an acceleration voltage of 80 kV. TEM samples were prepared by drop casting diluted solution of nanoparticles on Formvar coated Cu TEM grids (Plano).

Results and discussion

Peak broadening and crystallite size

The crystal structure of all nanoparticle anodes samples was investigated with XRD before and after cycling. Charge/discharge curves and cycle *versus* capacity graphs are added into the ESI.† The XRD measurements of the cycled electrodes can be seen in Fig. 1.

All nanoparticle samples show discrete reflections from the tetragonal β-Sn phase and two sharp reflections from the copper foil. The β-Sn reflections broaden toward smaller crystallite sizes. Electrodes with particles sizes from 23 nm to 15 nm show additionally broader reflections at 24°, 39° and 47°, which can be attributed to the cubic α-Sn structure. Their relative intensity (compared to the signals originating from β-Sn) increases for decreasing size of the particles.

We used the standard Williamson–Hall (W.–H.) analysis to determine the size of the crystallites and the strain of the nanoparticles. This analysis presupposes that the line broadening B depends on the size of the crystalline domain L (eqn (1)) and the inhomogeneous strain ε (eqn (2)):

$$B_{\mathrm{L}} = \frac{K\lambda}{L\cos(\theta)} \quad (1)$$

$$B_{\mathrm{e}} = 4\varepsilon\tan(\theta) \quad (2)$$

K is the Scherrer constant (for Sn 1.07)[22] and θ the angle from the 2θ-scan. The total broadening is the sum of eqn (1) and (2).

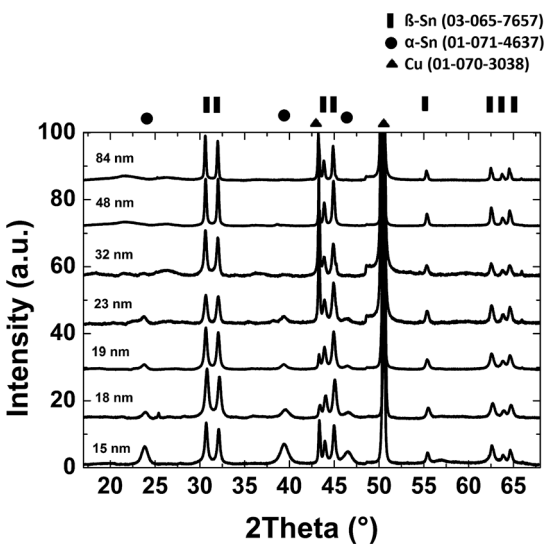

Fig. 1 XRD measurements of different sized Sn nanoparticle electrodes on copper foil after 10 cycles in a lithium-ion cell. The phases, giving rise to the observed reflections, are indicated.

$$B_{tot} = B_e + B_L = 4\varepsilon \tan(\theta) + \frac{K\lambda}{L\cos(\theta)}$$
$$B_{tot}\cos(\theta) = 4\varepsilon \sin(\theta) + \frac{K\lambda}{L} \quad (3)$$

By transformation of eqn (3) we get an expression, which allows us to separate the influence of the size of the crystallite L and the strain ε by measuring the profile broadening as a function of θ.

Fig. 2a shows the XRD pattern of the 15 nm sized Sn nanoparticle electrode, before and after cycling in a lithium-ion cell, the corresponding Williamson–Hall plot of the pattern is shown in Fig. 2b. A linear fit determines the size of the crystallites L (intercept) and the inhomogeneous strain ε (slope) of the crystallites. The reflections from the α-Sn structure are broader than the ones from the β-Sn phase. Before cycling, the Williamson–Hall analysis delivers 11(2) nm for the β-Sn crystals. After cycling, this analysis delivers 17(6) nm for the β-Sn structure and 8(1) nm for the new α-Sn structure.

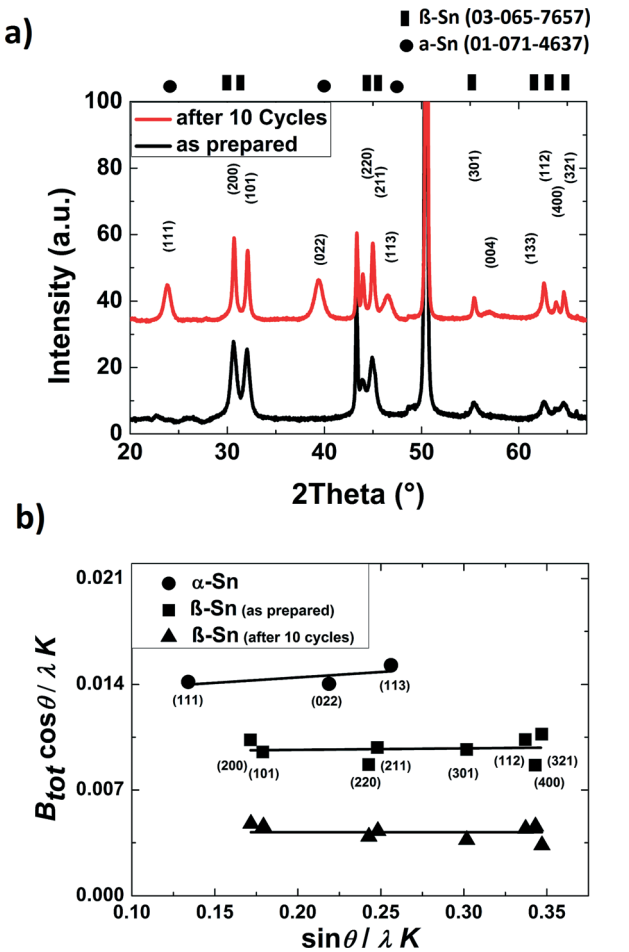

Fig. 2 a) XRD pattern of a 15 nm sized Sn nanoparticle electrode before and after cycling in a lithium-ion cell b) corresponding Williamson–Hall analysis of the integral peak width from Fig. 2a. The size of the β-Sn crystals from this analysis before cycling is 11(2) nm. After 10 cycles in the lithium-ion cell, the size of the β-Sn crystals increases to 17(6) nm. Reflections from α-Sn have a crystallite size of 8(1) nm.

Therefore, we assume that the smallest particles of the particle-distribution were transformed into the α-structure while the larger particles of this distribution retain the β-structure. The strain (slope) of the crystallites is small in all Williamson–Hall plots and was therefore not considered further.

Quantitative analysis

In powder XRD patterns, there is a linear dependency between the peak intensity ratio I_α/I_β and the weight ratio w_α/w_β (eqn (4)).[23]

$$\frac{I_\alpha}{I_\beta} = X\frac{w_\alpha}{w_\beta} \quad (4)$$

X is a constant and can be calculated (eqn (5)) from the relative intensity ratio (RIR) values, which are listed in the literature (ICDD Database).

$$X = \frac{\mathrm{RIR}_\alpha}{\mathrm{RIR}_\beta} \quad (5)$$

For α-Sn (01-071-4637) this value is 16.65 and for β-Sn (03-065-7657) 10.88. The proportionality constant X is therefore 1.53. With eqn (4) and the ratio of the integrated intensities, we calculated the weight ratio of α-/β-Sn for all nanoparticle electrodes, which show reflections from α-Sn structure.

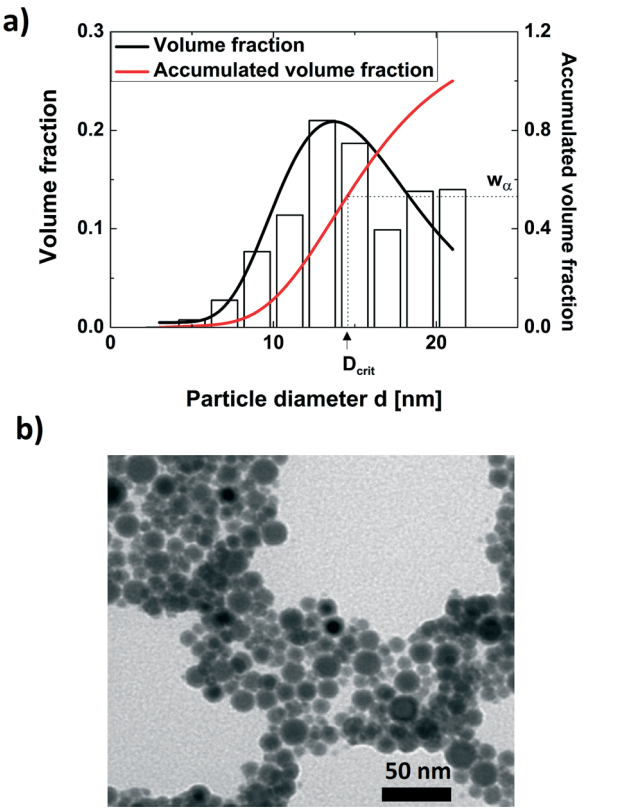

Fig. 3 a) Volume weighted size-histogram of a nanoparticle sample with a volume weighted mean diameter of 15 nm b) corresponding TEM image.

Fig. 3 shows the volume weighted size histogram together with the cumulative sum and the corresponding TEM image of the 15 nm particle sample.

The size histograms were determined by measuring one hundred particles from the as synthesized samples. With eqn (4) and the XRD measurement, we calculated the amount (wt%) of α-Sn structure in this sample to be 50%. Assuming that only the smallest particles in this distribution were transformed into α-Sn structure, we can determine a critical size for the transformation. Therefore, the cumulative sum at 50% delivers a critical particle size of 14(3) nm. That means, for this particle distribution, particles smaller 14 nm are transformed in the α-structure and particles larger than 14 nm remain in the β-structure.

We determined this critical size for all Sn electrodes with α-Sn structure content. Fig. 4 shows the amount of α-Sn with respect to the volume weighted particle size $D_{4,3}$. The inset of Fig. 4 shows the calculated critical size for the β- to α-transformation for all four nanoparticle samples, which show α-Sn reflections.

The mean critical size for the transformation from β- to α-structure is 17(4) nm. All measured and calculated parameters were summarized in Table 1.

Because all the samples were kept at room temperature, the presence of α-Sn in the nanoparticle electrodes is not expected.

Generally, the formation of α-Sn is a slow process, starting below 13.2 °C. The transformation from α-Sn back to β-Sn usually occurs at 32 °C. Metastability and hysteresis with respect to temperature and pressure are the result of the small difference in chemical free energy between the α- and β phases (at absolute zero temperature 0.022 eV per atom).[20] Nanoparticles can adopt a new structure in order to lower the total energy.[6] The dependency of the enthalpy with particle size was successfully calculated for Al_2O_3 [6] and TiO_2.[4] However, phase transformation can be induced by defects and pressure as well.[5] Therefore, for the Sn/SnO_x core/shell nanoparticles in this study, the complex interactions between surface energy, Li impurities and shell material makes an additional theoretical interpretation of these findings difficult.

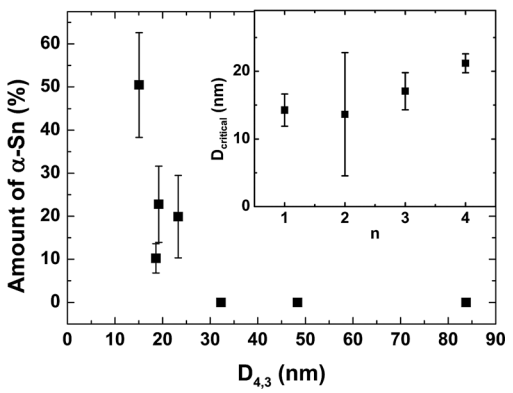

Fig. 4 Plot of the size of the particles *versus* the amount of α-Sn formed during lithium insertion/extraction. The inset shows the critical sizes for the β-α-transformation (calculated from the four samples which show α-Sn reflections). The assumption that only the smallest particles were transformed in the α-Sn structure is supported by different observations. First, α-Sn is only present in nanoparticle samples with mean particles sizes smaller or equal to 23 nm. Secondly, the Williamson–Hall analysis of the XRD peak broadening indicates, a change in the size distribution of the nanocrystals after lithium insertion/extraction. Compared with the original size of the crystallites before lithium insertion/extraction, β-Sn crystals are larger after the cycling procedure, while the new α-Sn crystals are always smaller than the original β-Sn crystals. These phenomena can be observed in all nanoparticle samples which show α-Sn reflections.

Temperature-dependence of the α-Sn structure

Temperature dependent XRD measurements were performed to determine the stability of the α-phase. Fig. 5b shows a clipping of the XRD pattern in the 2Theta range between 22° and 42°.

The temperature was increased in 10 °C steps per hour. Surprisingly, reflections originating from the α-phase can be found in the diffraction patterns measured at temperatures up to 220 °C. That is 10 °C above the melting point of the β-Sn nanoparticles. The melting point of nanoparticles is a function of their size and decreases towards smaller diameters.[24]

Considering the bulk phase diagram of pure tin, we would not expect such stability of the α-phase and its direct transition to the liquid phase.

Some reports in literature claim that small amounts of impurity metals can either stabilize the β- or the α-phase. For example small amounts (0.6 wt%) of Si raise the α- to β-transformation point to 90 °C.[25] Fyhn *et al.* reported, that small (13–21 nm) and stable precipitates of α-Sn with a melting point of 200 °C were formed in a silicon matrix.[19]

One explanation for the stability of the α-phase in electrodes composed of Sn nanoparticles could be the stabilization by lithium impurities. Furthermore, a cubic Li_2O shell, which is probably formed during the first lithiation[26] could act as a stabilizing matrix. The phase diagram of nanoparticles differs from that of the bulk material. Therefore, phase transitions and alloy formation at the nano-scale cannot be predicted based on standard phase diagrams. The larger surface to volume ratio for smaller particles could be an explanation for the presence of a critical transformation size. Because of the substantial contribution of the surface energy, nano-scale alloys form easily, even for materials combinations that are immiscible in the bulk, if the diameter of the particles is small, while phase segregation is observed for larger sizes.[27,28] Thus, we expect the incorporation of lithium impurities into Sn nanoparticles only up to a critical size, above which phase segregation occurs, which explains the observed behavior.

Conclusions

In conclusion, Sn nanoparticles can be transformed from the metallic β-structure to the semiconducting α-structure after

Table 1 Summarized data for all investigated nanoparticle samples

Particle size from TEM	Quantitative analysis from XRD		Critical size for β to α transformation	W.–H. analysis (as prepared)	W.–H. analysis (after 10 cycles)	
$D_{4,3}$[a] (nm)	$w_{a\text{-}Sn}$[b] (%)	$w_{\beta\text{-}Sn}$[c] (%)	D_{crit}[d] (nm)	$D_{\beta\text{-}Sn}$[e] (nm)	$D_{a\text{-}Sn}$[f] (nm)	$D_{\beta\text{-}Sn}$[g] (nm)
15.1	50(13)	50(13)	14(3)	11(2)	8(1)	17(6)
18.6	10(4)	90(4)	14(10)	14(2)	10(3)	22(3)
19.2	23(9)	77(9)	17(3)	16(5)	10(4)	18(3)
23.3	20(10)	80(10)	21(2)	21(4)	13(4)	23(2)
32.3	0	100	—	25(4)	—	26(4)
48.4	0	100	—	42(3)	—	45(3)
83.8	0	100	—	73(10)	—	53(4)

[a] $D_{4,3}$ denotes the volume-weighted mean particle diameter calculated on the basis of the TEM measurements according to $D_{4,3} = \frac{\sum d^4}{\sum d^3}$. [b] $w_{\alpha\text{-}Sn}$ denotes the amount of α-Sn in the sample. [c] $w_{\beta\text{-}Sn}$ denotes the amount of β-Sn in the sample. [d] D_{crit} denotes the critical size for the α/β-transformation. [e] $D_{\beta\text{-}Sn}$ denotes the size of the crystallite of β-Sn determined by XRD Williamson–Hall analysis. [f] $D_{\alpha\text{-}Sn}$ denotes the size of the crystallite of α-Sn determined by XRD Williamson–Hall analysis after lithium insertion/extraction. [g] $D_{\beta\text{-}Sn}$ denotes the size of the crystallite of β-Sn determined by XRD Williamson–Hall analysis after lithium insertion/extraction.

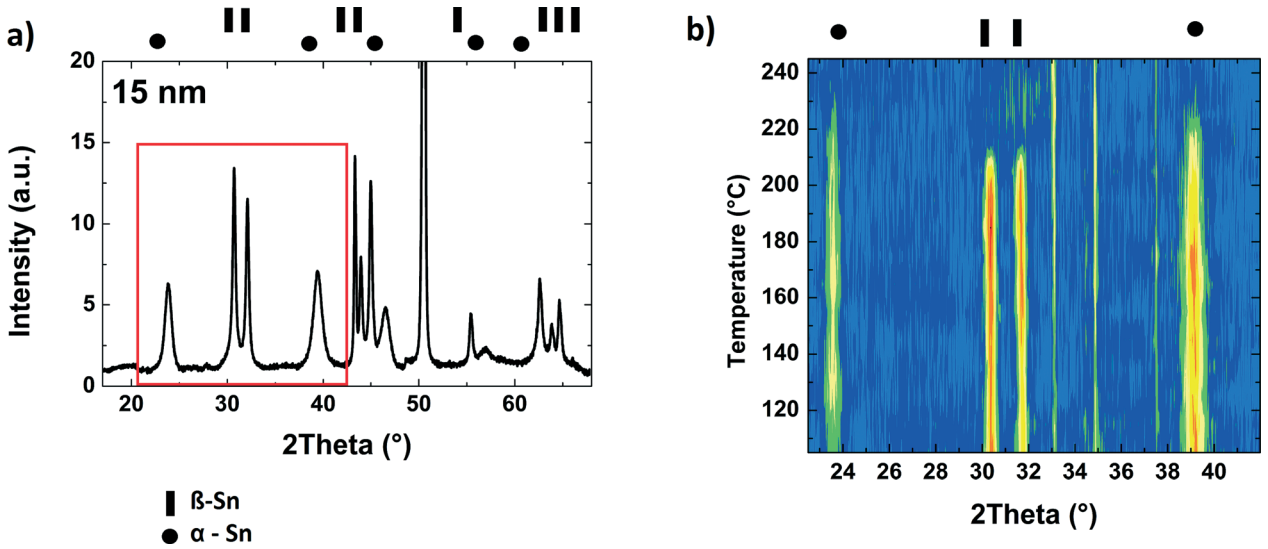

Fig. 5 a) XRD pattern of a 15 nm sample, consisting of 50 wt% α-Sn b) clipping of temperature depending XRD measurement. Small reflections at 33° and 35° 2Theta originate from the sample holder inside of the heating chamber.

lithium insertion and extraction. The critical size for this transformation is 17(4) nm. Temperature dependent XRD measurements on this phase yield a melting point of 220 °C. This phase transition from the α-phase to the liquid phase is not expected from the bulk phase diagram of pure tin. One explanation for this behavior could be small amounts of lithium impurities, which are stabilizing the α-phase. Also the Li_2O shell, which is formed during the first lithiation, could stabilize this phase (matrix-stabilization). Nevertheless, the larger surface to volume ratio with the substantial contribution of the surface energy can cause formation of alloys, which differ from that observed in the bulk materials.

Most likely, the internal electrical resistance of the electrode will increase, after a metal to semiconductor transformation. Nevertheless, smaller nanoparticle electrodes are showing the best cycling stabilities. Suitable tin alloys might prevent this phase transformation and should therefore be able to generate a high cycling stability in combination with a low electrical resistance. How these effects are affecting the electrochemical performance of a tin nanoparticle anode needs to be investigated in future works.

Acknowledgements

The authors gratefully acknowledge funding of the EWE-Nachwuchsgruppe by EWE AG Oldenburg and the EWE Research Centre NEXT ENERGY for laboratory equipment.

Notes and references

1 Q. Jiang, L. H. Liang and D. S. Zhao, *J. Phys. Chem. B*, 2001, **105**, 6275–6277.

2 N. Oehl, P. Michalowski, M. Knipper, J. Kolny-Olesiak, T. Plaggenborg and J. Parisi, *J. Phys. Chem. C*, 2014, **118**, 30238–30243.
3 A. A. Gribb and J. F. Banfield, *Am. Mineral.*, 1997, **82**, 717–728.
4 H. Zhang and J. F. Banfield, *J. Phys. Chem. B*, 2000, **104**, 3481–3487.
5 L. Piot, S. Le Floch, T. Cornier, S. Daniele and D. Machon, *J. Phys. Chem. C*, 2013, **117**, 11133–11140.
6 J. M. McHale, A. Auroux, A. J. Perrotta and A. Navrotsky, *Science*, 1997, **277**, 788–791.
7 S. Ram, *Mater. Sci. Eng., A*, 2001, **304–306**, 923–927.
8 Y. Sun, Y. Ren, Y. Liu, J. Wen, J. S. Okasinski and D. J. Miller, *Nat. Commun.*, 2012, **3**, 971.
9 J. Diao, K. Gall and M. L. Dunn, *Nat. Mater.*, 2003, **2**, 656–660.
10 M. Winter and J. O. Besenhard, *Electrochim. Acta*, 1999, **45**, 31–50.
11 X.-L. Wang, M. Feygenson, M. C. Aronson and W.-Q. Han, *J. Phys. Chem. C*, 2010, **114**, 14697–14703.
12 G. Schmuelling, N. Oehl, M. Knipper, J. Kolny-Olesiak, T. Plaggenborg, H.-W. Meyer, T. Placke, J. Parisi and M. Winter, *Nanotechnology*, 2014, **25**, 355401.
13 K. J. Rhodes, R. Meisner, M. Kirkham, N. Dudney and C. Daniel, *J. Electrochem. Soc.*, 2012, **159**, A294–A299.
14 C. Kim, M. Noh, M. Choi, J. Cho and B. Park, *Chem. Mater.*, 2005, **17**, 3297–3301.
15 L. Xu, C. Kim, A. K. Shukla, A. Dong, T. M. Mattox, D. J. Milliron and J. Cabana, *Nano Lett.*, 2013, **13**(4), 1800–1805.
16 Y. Kariya, N. Williams, C. Gagg and W. Plumbridge, *JOM*, 2001, **53**, 39–41.
17 M. Leodolter-Dworak, I. Steffan, W. J. Plumbridge and H. Ipser, *J. Electron. Mater.*, 2010, **39**, 105–108.
18 W. J. Plumbridge, *J. Electron. Mater.*, 2008, **37**, 218–223.
19 M. F. Fyhn, J. Chevallier, A. N. Larsen, R. Feidenhans and M. Seibt, *Phys. Rev. B: Condens. Matter Mater. Phys.*, 1999, **60**, 5770.
20 F. Vnuk, A. D. Monte and R. W. Smith, *J. Appl. Phys.*, 1984, **55**, 4171–4176.
21 G. Zeng, S. D. McDonald, Q. F. Gu, K. Sweatman and K. Nogita, *Philos. Mag. Lett.*, 2013, **94**, 53–62.
22 J. I. Langford and A. J. C. Wilson, *J. Appl. Crystallogr.*, 1978, **11**, 102–113.
23 C. R. Hubbard and R. L. Snyder, *Powder Diffr.*, 1988, **3**, 74–77.
24 E.-H. Kim and B.-J. Lee, *Met. Mater. Int.*, 2009, **15**, 531–537.
25 W. M. T. Gallerneault, F. Vnuk and R. W. Smith, *J. Appl. Phys.*, 1983, **54**, 4200–4201.
26 N. Li and C. R. Martin, *J. Electrochem. Soc.*, 2001, **148**, A164–A170.
27 H. You, S. Yang, B. Ding and H. Yang, *Chem. Soc. Rev.*, 2013, **42**, 2880–2904.
28 J. Li, M. Bloemen, J. Parisi and J. Kolny-Olesiak, *ACS Appl. Mater. Interfaces*, 2014, **6**, 20535–20543.

